Microstructural Evaluation of Ni-graphite Composites Sintered from NiO-SiC Powder Mixtures

Ella Raquel do Vale Souza de Lima[a], Armando Monte Mendes[a], Gisele Hammes[b] [ID],

Cristiano Binder[b], Aloisio Nelmo Klein[b], Antonio Eduardo Martinelli[a]* [ID]

[a]*Universidade Federal do Rio Grande do Norte, Departamento de Engenharia de Materiais, Natal, RN, Brasil.*
[b]*Universidade Federal de Santa Catarina, Departamento de Engenharia Mecânica, Florianópolis, SC, Brasil.*

Nickel alloys and composites are interesting engineering materials as a result of a combination of mechanical, corrosion and wear resistance at service temperatures that exceed those of steels and steel-based materials. The present study aimed at sintering Ni-graphite composites from NiO-SiC mixtures and investigate the *in-situ* formation of graphite. NiO powders were mixed with SiC (0, 3, 5 and 10 wt.%) and attrition-milled during 1 h. The mixtures were then granulated using 1.5 wt.% paraffin in hexane solution and uniaxially pressed under 400 MPa. The cylindrical pellets were then sintered at 1200 ºC. The sintered materials were characterized by density measurements, dilatometric and microstructural analyses, as well as Vickers microhardness. The results showed that Ni-graphite composites were successfully produced from NiO-SiC mixtures with full reduction of NiO and dissociation of SiC to form a Ni-Si matrix and graphite nodules.

Keywords: *Nickel composites, NiO, SiC, Graphite.*

1. Introduction

Nickel-based materials have been developed to be used as alloys and also as composites in applications for the automotive, petrochemical, food processing, aerospace and nuclear industries[1-4] where a combination of properties such as high mechanical strength, corrosion and wear resistance at high temperatures are required[1,5-9] Nickel presents considerable solubility to a variety of alloying elements such as Cr, Mo, W, Nb, Fe, Cu, Al, as well as Si[10-12]. In particular, the literature shows that the addition of Si to Ni increases hardness[13], but also decreases the solubility of carbon[14].

Particulate ceramics have been added to Ni matrices, usually as reinforcements to produce composites. Examples include Al_2O_3, TiO_2 and SiO_2 that are commonly added to improve the mechanical properties at both room and high temperatures, and the corrosion resistance[15-18]. Covalent ceramics such as nitrides, *e.g.,* TiN, and BN[19,20], borides, *e.g.,* TiB_2[19], carbides, *e.g.,* TiC, WC, NbC and SiC[21-24], in addition to elementary materials, such as C in the form of graphite[9] have also been used to improve the mechanical properties and tribological behavior.

Despite the high thermal and chemical stability of ceramic materials, some of them can undergo solubilization in metal matrices under suitable heat-treatment conditions. Backhaus-Ricoult[25] studied the solid-state reactions between SiC and various (Fe, Cr, Ni)-alloy compositions. These reactions can be attributed to the dissolution of SiC in Fe and Ni, resulting in the formation of Si-rich compounds (α-, τ-phase, Ni_5Si_2 or Ni_2Si) and graphite flakes. The presence of Cr results in large precipitates of Cr-carbide in the alloy. The dissociation of SiC particles yields the *in-situ* formation of graphite that

may act as a solid lubricant phase. This process has been extensively studied mostly in Fe-matrix materials, where Fe-Si-C compounds have been observed and resulted in superior tribological properties[26-31]. The solubilization of SiC in Ni matrix has been described by fewer authors. Parucker and Klein[32], for instance, reported the development of Ni alloys using carbides (SiC and WC) as sources of Si, W and C by powder metallurgy. The dissociation of SiC, followed by the formation of Ni-Si solid solution which increases the strength of the matrix, or intermetallic phases[25,33,34] depending on the heat-treatment conditions, and carbon-based precipitates[20,22]. Upon sintering, graphite phases remain stable in the final microstructure of the material[4,25].

Ni-based materials are commonly manufactured by methods such as casting, forging and powder metallurgy[6] using Ni powder. For the latter, fine particulates are used to promote adequate mixing and homogeneous phase distribution in the final microstructure. An alternative route to produce Ni-based composites consists in the use of NiO as starting powder. NiO can be easily reduced by hydrogen at low temperatures without polluting the environment, offering the potential for green energy use and generating only water vapor as byproduct, representing a direct method for preparing metals with uniform composition[35-37].

Therefore, the present study focused on the process route to obtain Ni-graphite composites from NiO-SiC powder mixtures. The effect of NiO reduction and the dissociation of SiC in the final microstructure were addressed. Ni matrix composites containing graphite nodules are expected to exhibit solid lubricant properties that improve wear resistance and reduce friction at higher service temperatures, exceeding the capabilities of Fe-based materials.

*e-mail: martinelli.ufrn@gmail.com

2. Experimental

NiO (D_{50} = 11.7 μm, > 98% pure) and SiC (D_{50} = 13.8 μm, 97.5% purity) particles were previously analyzed by X-ray diffraction (XRD) and Field-Emission Scanning Electron Microscopy (FEG-SEM). Mixtures containing 3, 5 and 10 wt% SiC were mixed with isopropyl alcohol in an attritor type mill at 200 rpm for 1 hour. After drying at ~ 100 °C for about 2 hours, pure NiO and NiO-SiC mixtures were granulated using 1.5 wt.% paraffin diluted in hexane in an ultrasound bath for 30 min. Commercially available paraffin lentils and hexane were used to granulate the feedstocks. The granules were classified using 500 to 90 μm sieves, and uniaxially pressed under 400 MPa for 1 min into cylindrical samples having 10 mm in diameter.

Three samples of each composition were sintered in a dilatometer (Netzsch, DIL 402) in the presence of 95% Ar + 5% H_2. The heating rate from room temperature to 500 °C was 5 °C/min. The samples remained at 500 °C during 1 hour for the removal of the binder and then heated up to 1200 °C at 5 °C/min for a 1-hour sintering cycle. The samples were naturally cooled down under flowing gas. The sintered samples were named according to the starting percentage of SiC. Thus, contents of 0, 3, 5 and 10 wt.% SiC are related to samples N0, N3, N5 and N10, respectively.

The green and sintered densities were measured by the geometrical method using a digital micrometer with resolution of 0.001 mm. The sintered samples were cut, and the resulting cross-sections were grinded with 180-1200 grit papers and polished using 1 μm alumina slurry and 0.3 μm diamond paste. The samples were then etched in marble solution. The microstructural characterization took place using optical microscopy (Olympus GX-51) and FEG-SEM (FEGSEM, Zeiss Auriga 40) equipped with an energy-dispersive X-ray spectrometer. The crystallographic phases were identified by X-ray diffraction (Bruker D8) with Cu-kα radiation (λ = 1.5418 Å). Vickers microhardness (Shimadzu HMV 2000) was measured according to ASTM E384 standard with primary load of 500 g and 25 g for 10-15 s for each indentation.

3. Results and Discussion

3.1. Starting powders and mixtures

Figure 1 shows the micrographs of NiO (a) and SiC (b) powders along with the corresponding XRD patterns. NiO particles presented irregular rounded morphology with some agglomeration and single NiO phase indexed to JCPDS No.89-7131, whereas SiC particles presented faceted morphology corresponding to a single SiC phase related to JCPDS No.31-1232.

The NiO-SiC mixtures were evaluated by SEM analyses (Figure 2). All mixtures presented a homogeneous distribution of SiC (some are highlighted in the image by circles) and NiO particles with few small agglomerations of particles (highlighted in the image by arrows).
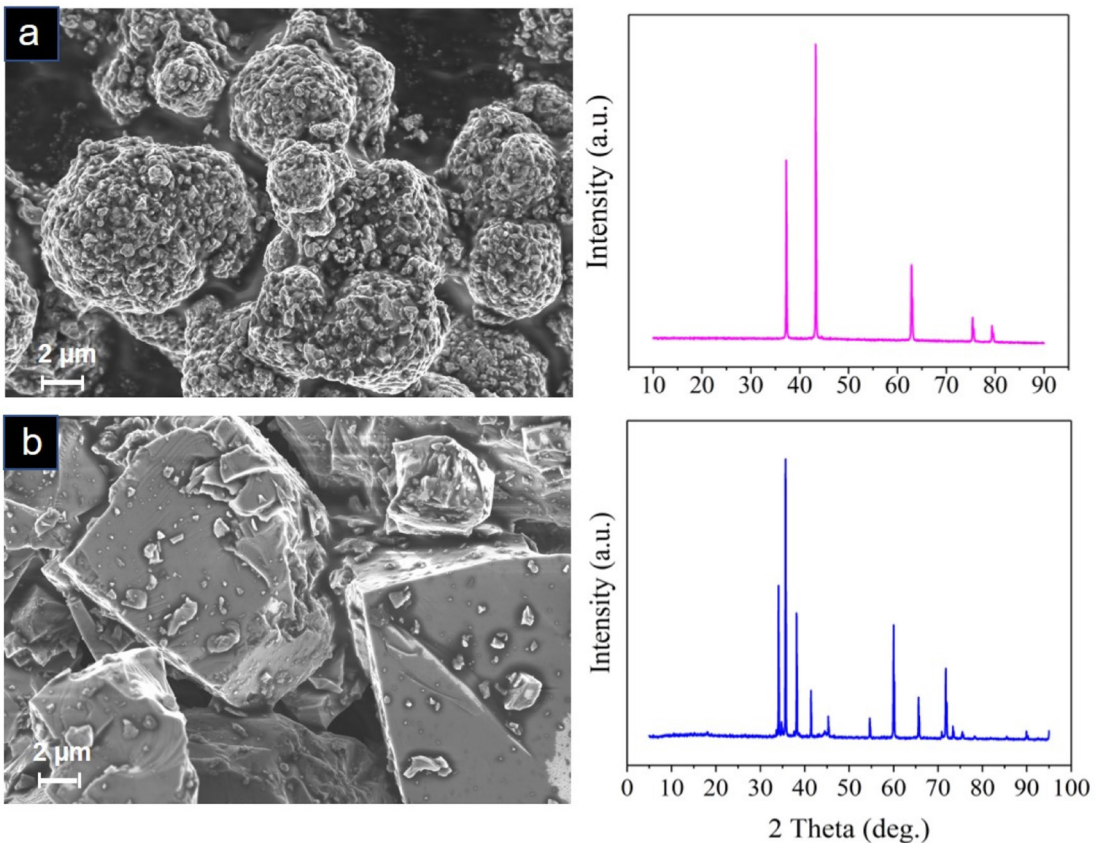

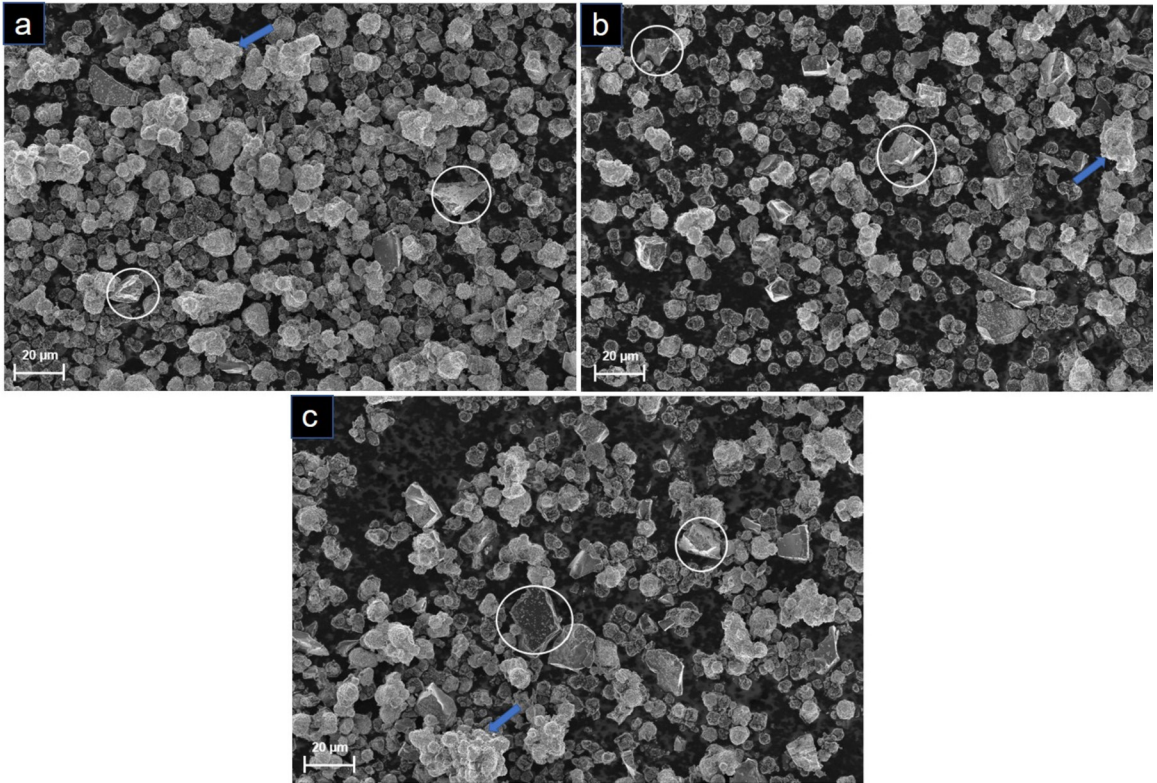**Figure 1.** SEM micrographs and XRD analyses of the starting (a) NiO; (b) SiC powders.

Figure 2. SEM micrographs of the NiO-SiC mixtures with different concentrations of SiC: (a) 3 wt.%, (b) 5 wt.% and (c) 10 wt.%.

3.2. Dilatometric analysis

The dilatometric behavior of the samples is shown in Figure 3. All samples depicted a shrinkage point at ~ 340 ºC - 360 ºC, related to the decomposition of paraffin. According to the literature, paraffin starts to decompose at around 210 °C, and is expected to fully evaporate at about 450 °C[38]. The plots for all compositions tested overlapped at ~500 ºC, and the shrinkage corresponded to the reduction of NiO, which started at around 400 ºC. This is in good agreement with the literature which states that, according to the Ellingham diagram[39], the reduction of NiO to Ni takes place starting at 420 ºC, with $\Delta G = -0.176$ kJ mol^{-1}. In addition, in the temperature range from 400 to 600 °C, the rate of reduction of NiO increases with increasing both temperature and hydrogen pressure[40]. The shrinkage rate increased in the range of 600 ºC - 700 ºC as most of the NiO was reduced. Full reduction under H_2 is expected to take place below 950 °C[36,39]. In fact, XRD results did not revealed the presence of NiO, however traces of oxygen were observed by EDS.

The onset of sintering took place at around 600 ºC, which is in good agreement with the literature[35,36]. Sample N3 showed continuous and uniform densification as the temperature increased, reaching ~ 27% shrinkage after 1 hour at 1200 °C (Figure 3b). The uniform distribution of SiC particles improved the densification of the matrix as well as the solubilization of Si in Ni[41]. On the other hand, compositions with 5 wt% of SiC, depicted a reduction in densification, probably due to a formation of a larger number of graphite nodules. Sample N10, containing the highest

content of SiC, depicted slower sintering rate until around 1100 ºC, compared to the others, which may be due to the dissociation of higher relative contents of SiC. In addition, above 700 ºC, metastable nickel silicide starts to form[33]. Furthermore, SiC particles are quite stable at low temperatures and may hinder the contact between Ni particles[29]. The shrinkage of sample N10 improved above ~1150 ºC. From the Ni-Si phase diagram, liquid phase is expected to form in the range of 15 to 22 at. % Si, above 1143 ºC[33].

3.3. Microstructural evaluation of sintered samples

XRD patterns of all samples are shown in Figure 4. There was virtually complete reduction of the NiO matrix and removal of the binder. The mixtures containing various concentrations of SiC showed pure Ni (ICSD nº 64989) and graphite C (ISCD nº 88810). The fcc structure of the Ni matrix did not change with the addition of 3%, 5% or 10% wt.% SiC. There was a slight displacement of the Ni peaks due to the presence of Si in solid solution in the nickel matrix. Peaks at $2\theta = 26.6°$ correspond to the (002) planes of hexagonal graphite, resulting from the dissociation of SiC in the nickel matrix[42]. Sample N10 also revealed the presence of cubic Ni_3Si (ICSD nº 76413).

Optical micrographs of plain Ni and Ni-SiC samples are shown in Figure 5. The Ni matrix (Figure 5a) is characterized by equiaxial grains, twin boundaries (indicated with arrows) and pores. It is not straightforward to differentiate pores from graphite nodules solely by micrographs, as they both present dark contrast in the metal matrix. Samples containing SiC depict pores and graphite nodules. Comparing Figure 5a with
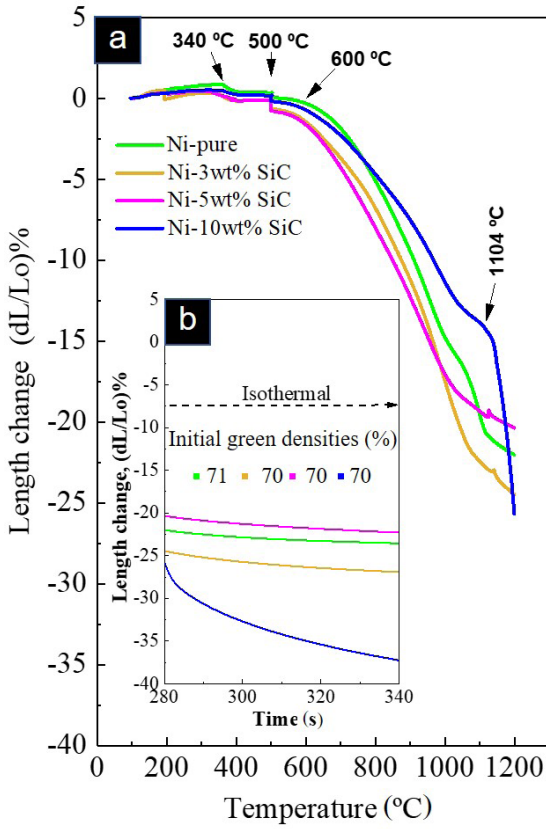
Figure 3. Dilatometric analyses for the sintering of Ni-based samples with length variation as a function of (a) temperature and (b) time (isothermal at 1200 °C).

the others, it is possible to see the typical morphology of pores and graphite nodules, which appear to be more elongated and irregular than the pores. Confirmation of this can be seen in the electron microscopy image in Figure 6, which shows the EDS of a porous region and a graphite nodule. All samples depicted the presence of pores intergranular and intragranular (regions indicated with circles) and clearly seen in Figure 5a. Areas attributed to graphite nodules increased with the concentration of SiC. According to Bougiouri[14], the addition of Si to Ni significantly decreases the solubility of carbon in nickel. High concentrations of carbon promote large amounts of agglomerates[43].
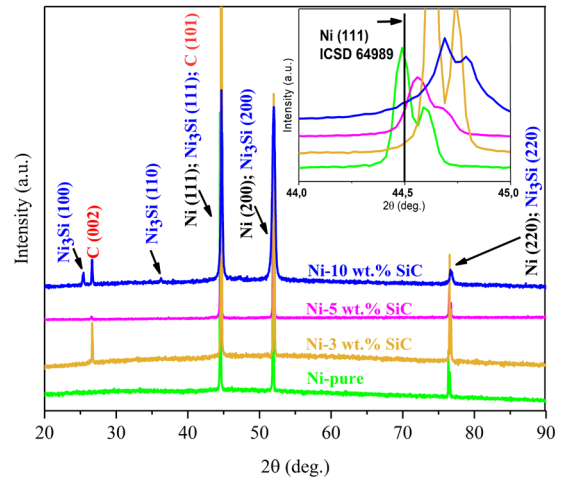

Figure 4. XRD patterns of the powders pure Ni and composite the Ni with different wt.% SiC sintered at 1200 °C.
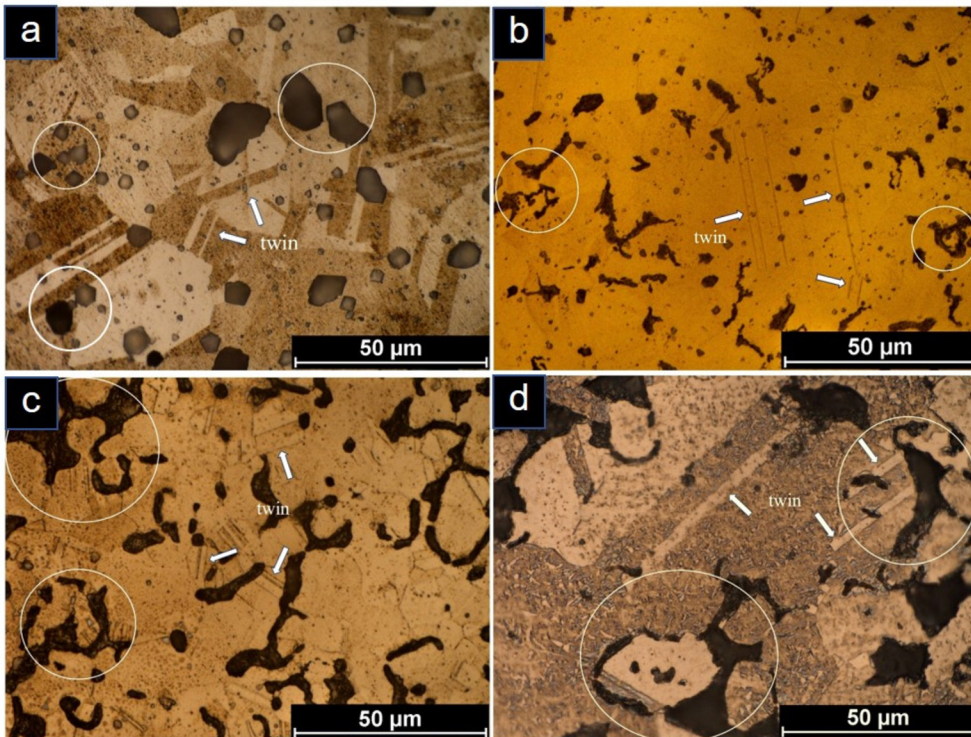

Figure 5. Optical micrographs after etching: (a) pure Ni, (b) Ni-3 wt.% SiC, (c) Ni-5 wt.% SiC and (d) Ni-10 wt.% SiC.
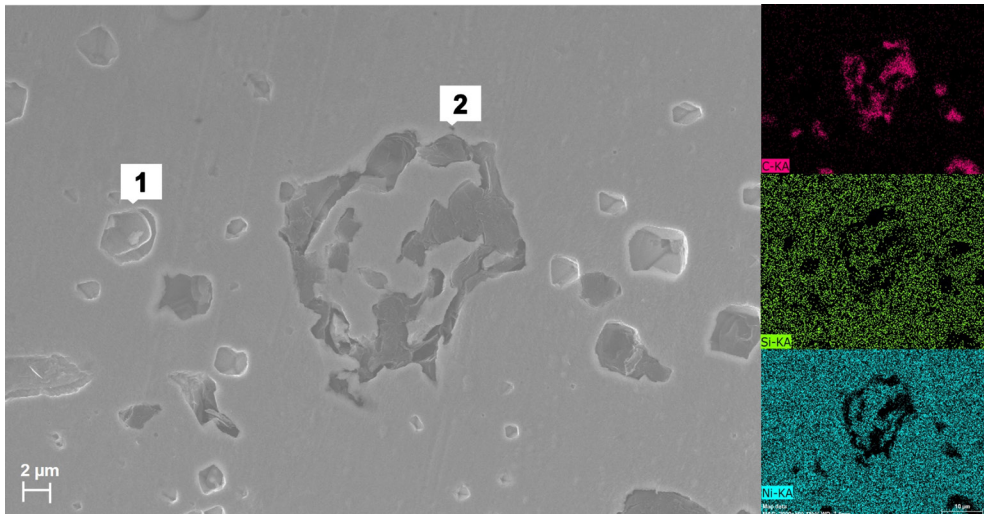
Figure 6. Micrograph analysis by SEM-EDS and mapping using EDS of different morphological phases in the Ni-3 wt.% SiC composite sintered at 1200 °C: (1) discontinuities of solid solution of Si and C in Ni (FCC) (2) carbon agglomerates.

The combination of SEM micrographs with EDS mapping of sample N3 is shown in Figure 6. Ni and Si are quite uniformly dispersed.

The microstructure and EDS profile of sample N10 are shown in Figure 7. In Figure 7a, the arrow indicates the direction from the border to the center of the sample. The change in grain morphology is evident. The composition of sample N10 (Ni – 10 wt.% SiC) lies in the region consisting of a Ni-Si solid solution, carbon in the form of graphite, and a NiSi liquid phase (Figure 7a). According to the Ni-Si-C phase diagram at 1200 °C[33], concentrations of Si between 7 and 10 wt.% yield the formation of Ni-Si solid solution and a liquid phase. The solid/liquid interfaces result in grains with dendritic morphology, as shown in Figure 7b. The region labelled (1) in Figure 7a contains approximately 85 wt.% Ni, 7.5 wt.% Si, corresponding to the Ni matrix with Si in solid solution and some carbon. The composition of the matrix (labelled (2)) contains 77.0 wt.% Ni, 12.0% Si which is related to the Ni_3Si intermetallic phase and approximately the same amount of carbon. Phase labelled (3) is essentially carbon. Region labelled (4) also shows high concentration of carbon, along with some Si and Ni, probably from adjacent matrix grains. Residual oxygen was identified in the samples, which may be attributed to the presence of residual NiO as well as the formation of oxides during metallographic preparation. Nevertheless, the remaining oxide fraction is small, to the extent that it does not interfere with the properties of the materials.

3.4. Densification of Ni-SiC composites

The green, sintered and theoretical densities of Ni-SiC based materials are shown in Figure 8a. The densities of green samples containing NiO, SiC and 1.5 wt.%. paraffin, presented subtle reduction with increasing SiC content. The same behavior was observed after sintering, for compositions with up to 10 wt.% SiC, due to the difference between the density of Ni (9.8 g/cm³) and SiC (3.2 g/cm³). Higher concentrations of SiC resulted in graphite clusters and, therefore, reduced density.

The relative densities of of Ni-SiC based materials are shown in Figure 8b. The theoretical density of the material was calculated as a mixture of metallic nickel with SiC, considering the complete reduction of NiO to Ni and the initial mass of SiC. The green relative density of the compositions did not exceed 70%. There was no significant change in the relative green density with the increase in the concentration of SiC. The relative density of the samples after sintering were limited to 90%, depicted by the sample with 3 wt% SiC.

3.5. Hardness measurements

The results of the Vickers microhardness measurements are shown in Figure 9. It is visible that both the average and the standard deviation increased with increasing SiC contents (Figure 9a). Hardening by solid solution and hardening by precipitation are the main mechanisms that increase the hardness of nickel-based super alloys[44]. Twinning can also explain the increase in hardness in reinforced composites[42,45]. The increase in the average hardness was caused by the dissolution of SiC and the resulting formation of Ni-Si solid solution. Lattice distortion hindered the dislocation motion and increased hardness. Ni_3Si is also a hard phase[46], and its presence was confirmed by XRD analysis (Figure 4) for sample N10. The increase in standard deviation resulted from the presence of graphite precipitates throughout the microstructure of the composite, since indentation was randomly selected. The microhardness of the Ni matrix and graphite nodules were individually examined, by selecting the locations for the indentations and reducing the load from 500 g to 25 g (Figure 9b). The difference in microhardness is evident for all compositions. Comparing the results from Figure 9a and 9b, it can be seen that the former corresponds to an average of the two constituents of the composite. The hardness of the matrix is higher than that of the graphite nodules.
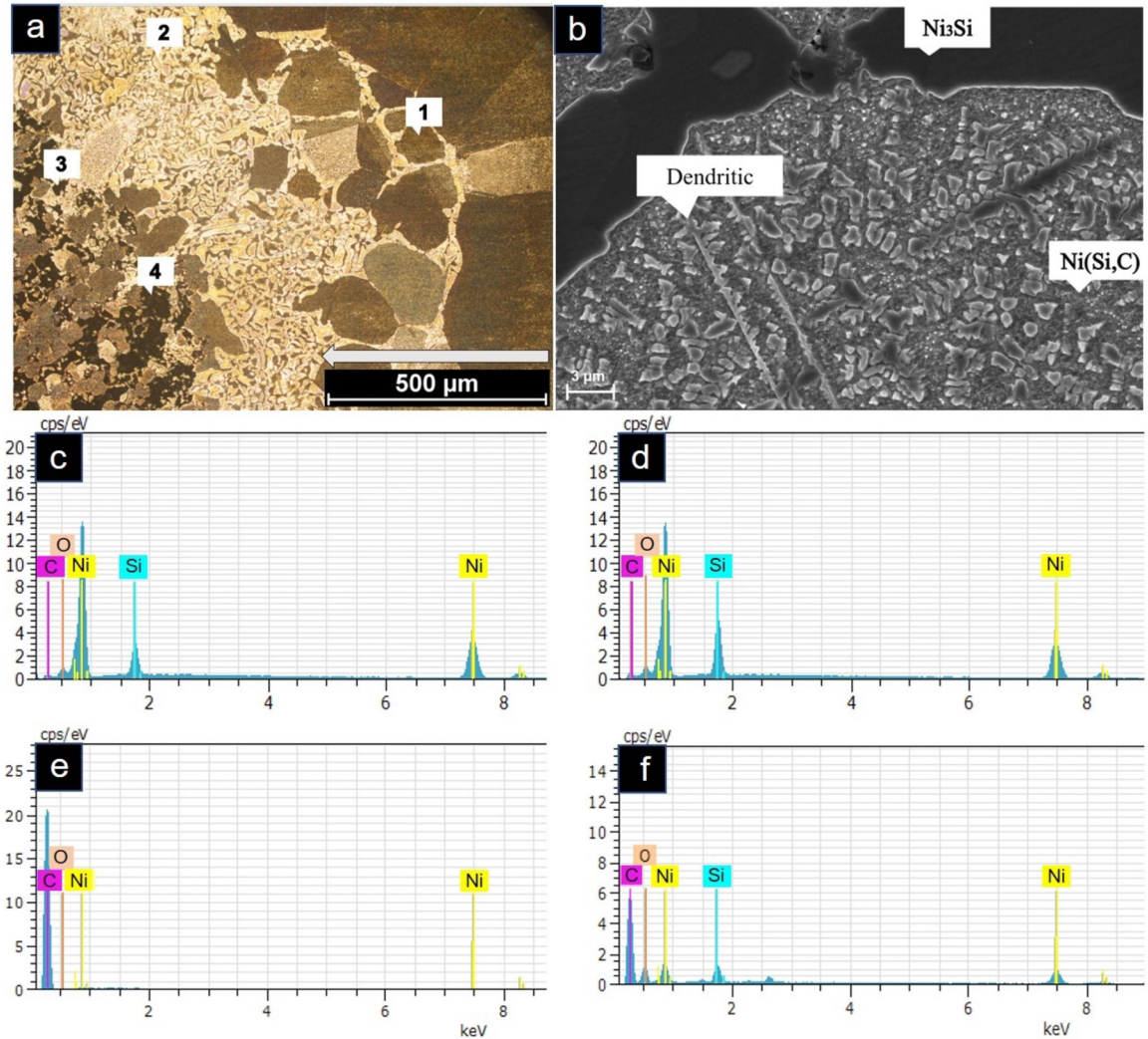
Figure 7. (a) Micrograph indicating different morphological phases in grains in the alloy composite Ni-10wt% SiC after sintered at 1200 °C; (b) SEM microstructure image; (c-f) EDS analyses of the areas 1, 2, 3 and 4, respectively.
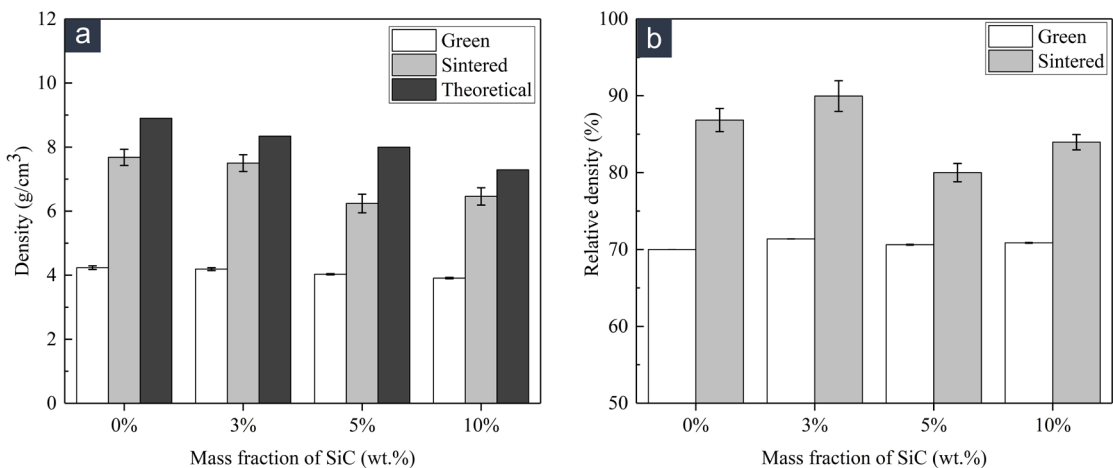

Figure 8. (a) Green, sintered and theoretical density of Ni-SiC based materials; (b) Relative densities.
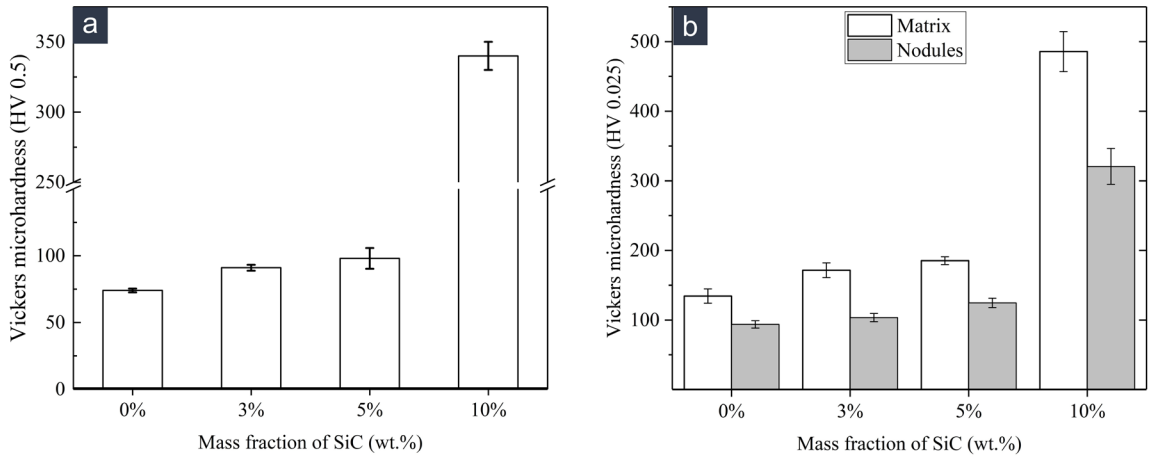
Figure 9. Vickers microhardness of (a) pure Ni and Ni-SiC composites and (b) Ni matrix and graphite nodules.

4. Conclusions

Ni-graphite composites were successfully produced from NiO-SiC mixtures. NiO was virtually fully reduced and the composites sintered after a single heat-treatment from room temperature to 1200 °C. SiC dissociated into Si and C.

NiO-SiC mixtures had a homogeneous distribution with some small NiO particle agglomerates.

Dilatometric analyses revealed shrinkage, sintering, and nickel silicide formation. Sample N3 exhibited continuous densification, while N10 showed rapid dimensional contraction due to the formation of a liquid phase.

XRD analysis confirmed the reduction of the NiO matrix and the presence of pure Ni and graphite phases. SiC addition did not significantly alter the Ni matrix structure. Si diffuses into Ni but does not significantly change the positions of the XRD peaks. In the sample containing 10% SiC, a new phase was formed. Graphite formation from the dissociation SiC was observed.

The density of Ni-based samples decreased as the SiC content increased. Higher SiC concentrations increased the formation of graphite nodules.

SiC-reinforced composites showed increased microhardness compared to pure Ni. Sample N3 had greater densification, while the sample with 10% SiC exhibited the highest hardness. Hardening mechanisms included solid solution and precipitation, with Ni_3Si phase confirmed in sample N10.

5. Acknowledgments

6. References

1. Deshpande YV, Andhare AB, Padole PM. How cryogenic techniques help in machining of nickel alloys? A review. Mach Sci Technol. 2018;22(4):543-84.

2. Sindhuja M, Sudha V, Haripriya S, Venugopal R, Usmani B. Electrodeposited Ni/SiC composite coating on graphite for high-temperature solar thermal applications. Mater Sci Energy Technol. 2018;1(1):3-10.

3. Nosonovsky M, Rohatgi PK. Biomimetics in materials science: self-healing, self-lubricating and self-cleaning materials. New York: Springer; 2012. 451 p.

4. Parucker ML, Klein AN, Binder C, Ristow W Jr, Binder R. Development of self-lubricating composite materials of nickel with molybdenum disulfide, graphite and hexagonal boron nitride processed by powder metallurgy: preliminary study. Mater Res. 2014;17(1):180-185.

5. Kiliç F, Gül H, Aslan S, Alp A, Akbulut H. Effect of CTAB concentration in the electrolyte on the tribological properties of nanoparticle SiC reinforced Ni metal matrix composite (MMC) coatings produced by electrodeposition. Colloids Surf A Physicochem Eng Asp. 2013;419:53-60.

6. Lei Y, Li X, Sun R, Tang Y, Niu W. Effect of sintering temperature and heat treatment on microstructure and properties of nickel-based superalloy. J Alloys Compd. 2020;818:152882.

7. Hrastnik K. United States patent US Appl. 10/448, 651. 2004.

8. Ulutan D, Ozel T. Machining induced surface integrity in titanium and nickel alloys: a review. Int J Mach Tools Manuf. 2011;51(3):250-80.

9. Hammood HS, Mahmood A, Irhayyim SS. Effect of graphite particles on physical and mechanical properties of nickel matrix composite. Period Eng Nat Sci. 2019;7(3):1318-28..

10. Klapper HS, Zadorozne NS, Rebak RB. Localized corrosion characteristics of nickel alloys: a review. Chin Shu Hsueh Pao. 2017;30:296-305.

11. Jena AK, Chaturvedi MC. The role of alloying elements in the design of nickel-base superalloys. J Mater Sci. 1984;19(10):3121-39.

12. Cheng S, Wang J, Wu Y, Qin X, Zhou L. Microstructure, thermal stability and tensile properties of a Ni–Fe–Cr based superalloy with different Fe contents. Intermetallics. 2023;153:107785.

13. Gulpen JH, Kodentsov AA, van Loo FJJ. Growth of silicides in Ni-Si and Ni-SiC bulk diffusion couples. Int J Mater Res. 1995;86(8):530-9.

14. Bougiouri V, Voytovych R, Dezellus O, Eustathopoulos N. Wetting and reactivity in Ni–Si/C system: experiments versus model predictions. J Mater Sci. 2007;42(6):2016-23.

15. Akhtar F. Synthesis, microstructure and mechanical properties of Al_2O_3 reinforced Ni_3Al matrix composite. Mater Sci Eng A. 2009;499(1-2):415-20.

16. Donnet C, Erdemir A. Historical developments and new trends in tribological and solid lubricant coatings. Surf Coat Tech. 2004;180-181:76-84.

17. Kumaraswamy J, Kumar V, Purushotham GG, Suresh R. Thermal analysis of nickel alloy/Al_2O_3/TiO_2 hybrid metal matrix composite in automotive engine exhaust valve using FEA method. Therm Eng. 2021;7(3):415-28.

18. Wang Y, Zhou Q, Li K, Zhong Q, Bui QB. Preparation of Ni–W–SiO_2 nanocomposite coating and evaluation of its hardness and corrosion resistance. Ceram Int. 2015;41(1):79-84.

19. Shokati AA, Parvin N, Shokati M. Combustion synthesis of NiAl matrix composite powder reinforced by TiB_2 and TiN particulates from Ni–Al–Ti–BN reaction system. J Alloys Compd. 2014;585:637-43.

20. Hu Z, Tong G. Laser sintered thin layer graphene and cubic boron nitride reinforced nickel matrix nanocomposites. In: AOPC 2015: Micro/Nano Optical Manufacturing Technologies; and Laser Processing and Rapid Prototyping Techniques; 2015; Beijing, China. Proceedings. Bellingham: SPIE; 2015. (vol. 967302).

21. Hu W, Huang Z, Cai L, Lei C, Zhai H, Zhou Y. Exploring the interfacial state and tensile behaviors in nickel matrix composite with in-situ TiC and γ'-Ni_3(Al,Ti) reinforcements. J Alloys Compd. 2018;765:987-93.

22. Wang W, Zhai H, Chen L, Huang Z, Bei G, Baumgärtner C, et al. Preparation and mechanical properties of in situ TiC_x–Ni (Si, Ti) alloy composites. Mater Sci Eng A. 2014;616:214-8.

23. Yin FS, Sun XF, Li JG, Guan HR, Hu ZQ. Preparation of a (Ti, Nb, W) C particulate reinforced nickel-base superalloy via super-high temperature treatment of melt. Mater Lett. 2003;57(22-23):3377-80.

24. Baron AF, Guerrero J, González JM, Gómez A, Jurado A, Sthepa HS. Effect of Ni content on the microstructure, thermal properties, and morphology of Ni-SiC composites produced by mechanical alloying. Ceram Int. 2017;43(2):2592-7.

25. Backhaus-Ricoult M. Solid state reactions between silicon carbide and (Fe, Ni, Cr) - alloys: reaction paths, kinetics and morphology. Acta Metall Mater. 1992;40:S95-103.

26. Mello JDB, Binder C, Hammes G, Klein AN. Effect of the metallic matrix on the sliding wear of plasma assisted debinded and sintered MIM self-lubricating steel. Wear. 2013;301(1-2):648-55.

27. Binder C, Bendo T, Pereira RV, Hammes G, Mello JDB, Klein AN. Influence of the SiC content and sintering temperature on the microstructure, mechanical properties and friction behaviour of sintered self-lubricating composites. Powder Metall. 2016;59(5):384-93.

28. Mello JDB, Binder C, Hammes G, Binder R, Klein AN. Tribological behavior of sintered iron based self-lubricating composites. Friction. 2017;5(3):285-307.

29. Binder C, Bendo T, Hammes G, Neves GO, Binder R, Mello JDB, et al. Structure and properties of in situ generated two-dimensional turbostratic graphite nodules. Carbon. 2017;124:685-92.

30. Mello JDB, Binder C, Binder R, Klein AN. Effect of precursor content and sintering temperature on the scuffing resistance of sintered self lubricating steel. Wear. 2011;271(9-10):1862-7.

31. Campos KR, Kapsa P, Binder C, Klein AN, Mello JDB. Tribological evaluation of self-lubricating sintered steels. Wear. 2015;332-333:932-40.

32. Parucker ML, Klein NA. Desenvolvimento de ligas sinterizadas de níquel para aplicações como matriz de materiais compósitos. Rev Eletron Mater Proc. 2014;9(1):16-21.

33. Du Y, Schuster JC. Experimental investigations and thermodynamic descriptions of the Ni-Si and C-Ni-Si systems. Metall Mater Trans, A Phys Metall Mater Sci. 1999;30(9):2409-18.

34. Yuan X, Zhang L, Du Y, Xiong W, Tang Y, Wang A, et al. A new approach to establish both stable and metastable phase equilibria for FCC ordered/disordered phase transition: application to the Al-Ni and Ni-Si systems. Mater Chem Phys. 2012;135(1):94-105.

35. Rhamdhani MA, Jak E, Hayes PC. Basic Nickel Carbonate: part I. Microstructure and phase changes during oxidation and reduction processes. Metall Mater Trans, B, Process Metall Mater Proc Sci. 2008;39(2):218-33.

36. Jeangros Q, Hansen TW, Wagner JB, Damsgaard CD, Dunin-Borkowski RE, Hébert C, et al. Reduction of nickel oxide particles by hydrogen studied in an environmental TEM. J Mater Sci. 2013;48(7):2893-907.

37. Hidayat T, Rhamdhani MA, Jak E, Hayes PC. On the relationships between the kinetics and mechanisms of gaseous hydrogen reduction of solid nickel oxide. Metall Mater Trans, B, Process Metall Mater Proc Sci. 2009;40(4):474-89.

38. Jaw KS, Hsu CK, Lee JS. The thermal decomposition behaviors of stearic acid, paraffin wax and polyvinyl butyral. Thermochim Acta. 2001;367-368:165-8.

39. Díaz SC, Garcés A, Restrepo OJ, Lara MA, Camporredondo JE. Thermodynamic analysis of the reduction process of Colombian lateritic nickel ore. Rev Metal. 2015;51(4):e057.

40. Utigard TA, Wu M, Plascencia G, Marin T. Reduction kinetics of Goro nickel oxide using hydrogen. Chem Eng Sci. 2005;60(7):2061-8.

41. Torres CS, Schaeffer L. Effect of high energy milling on the microstructure and properties of WC-Ni composite. Mater Res. 2010;13(3):293-8.

42. Wen T, Fan K, Zhang F. High strength and high ductility in nickel matrix nanocomposites reinforced by carbon nanotubes and onion-like-carbon hybrid reinforcements. J Alloys Compd. 2020;814:152303.

43. Damin KVS, Lucena AC, Bendo T, Klein NA, Binder C. Self-lubricating composites enriched in the surface with molybdenum and nickel. Mater Res. 2019;22(1, Suppl 1):e20180803.

44. Jiang S, Tian Z, Liu W, Chen H, Yang H, Liu Z, et al. Microstructural evolution and hardness of a heat resistant alloy during long term aging at 700 °C. J Alloys Compd. 2018;765:1267-74.

45. Hou Z, Xiong L, Liu Y, Zhu L, Li W. Preparation of super-aligned carbon nanotube reinforced nickel-matrix laminar composites with excellent mechanical properties. Int J Miner Metall Mater. 2019;26(1):133-41.

46. Amateau MF, Nicholson DW, Glaeser WA. Review of recent developments in the metallurgy of Beryllium. Columbus: Battelle Memorial Institute; 1961.